JCI insight

RESEARCH ARTICLE

AAV CRISPR editing rescues cardiac and muscle function for 18 months in dystrophic mice

Chady H. Hakim,[1,2] Nalinda B. Wasala,[1] Christopher E. Nelson,[3,4] Lakmini P. Wasala,[1] Yongping Yue,[1] Jacqueline A. Louderman,[1] Thais B. Lessa,[1] Aihua Dai,[1] Keqing Zhang,[1] Gregory J. Jenkins,[1] Michael E. Nance,[1] Xiufang Pan,[1] Kasun Kodippili,[1] N. Nora Yang,[2] Shi-jie Chen,[5,6] Charles A. Gersbach,[3,4,7] and Dongsheng Duan[1,8,9,10]

[1]Department of Molecular Microbiology and Immunology, School of Medicine, University of Missouri, Columbia, Missouri, USA. [2]National Center for Advancing Translational Sciences, NIH, Rockville, Maryland, USA. [3]Department of Biomedical Engineering and [4]Center for Genomic and Computational Biology, Duke University, Durham, North Carolina, USA. [5]Department of Physics and [6]Department of Biochemistry, University of Missouri, Columbia, Missouri, USA. [7]Department of Orthopaedic Surgery, Duke University Medical Center, Durham, North Carolina, USA. [8]Department of Neurology, School of Medicine, [9]Department of Bioengineering, and [10]Department of Biomedical Sciences, College of Veterinary Medicine, University of Missouri, Columbia, Missouri, USA.

Adeno-associated virus–mediated (AAV-mediated) CRISPR editing is a revolutionary approach for treating inherited diseases. Sustained, often life-long mutation correction is required for treating these diseases. Unfortunately, this has never been demonstrated with AAV CRISPR therapy. We addressed this question in the mdx model of Duchenne muscular dystrophy (DMD). DMD is caused by dystrophin gene mutation. Dystrophin deficiency leads to ambulation loss and cardiomyopathy. We treated 6-week-old mice intravenously and evaluated disease rescue at 18 months. Surprisingly, nominal dystrophin was restored in skeletal muscle. Cardiac dystrophin was restored, but histology and hemodynamics were not improved. To determine the underlying mechanism, we evaluated components of the CRISPR-editing machinery. Intriguingly, we found disproportional guide RNA (gRNA) vector depletion. To test whether this is responsible for the poor outcome, we increased the gRNA vector dose and repeated the study. This strategy significantly increased dystrophin restoration and reduced fibrosis in all striated muscles at 18 months. Importantly, skeletal muscle function and cardiac hemodynamics were significantly enhanced. Interestingly, we did not see selective depletion of the gRNA vector after intramuscular injection. Our results suggest that gRNA vector loss is a unique barrier for systemic AAV CRISPR therapy. This can be circumvented by vector dose optimization.

Introduction

CRISPR/Cas9-mediated genome editing is an emerging and revolutionary approach to treat human diseases. In this technology, the Cas9 endonuclease is directed to the intended location by the guide RNA (gRNA) to create a double-strand break. Subsequent DNA repair results in religation of the broken ends and genomic modifications at the target site. Duchenne muscular dystrophy (DMD) is a progressive degenerative disease affecting skeletal muscle and the heart in approximately 250–300,000 boys and young men worldwide. DMD is caused by out-of-frame mutations in the dystrophin gene. Recent studies suggest that delivery of CRISPR genome-editing tools by adeno-associated virus (AAV) can reframe the mutated dystrophin gene and restore dystrophin expression in DMD patient cells in vitro and in short-term mouse studies in vivo (1–11).

DMD is a chronic disease. A desirable therapy for DMD requires persistent, ideally lifelong, dystrophin restoration in both skeletal and cardiac muscle. Despite the encouraging proof-of-principle results from short-term studies (1–3, 7, 10), it is unclear whether a one-time systemic AAV CRISPR therapy can lead to long-term dystrophin restoration and disease amelioration. To address this critical issue, we injected AAV-9 CRISPR vectors via the tail vein to 6-week-old mdx mice, a widely used DMD model, and examined dystrophin expression and disease rescue at 18 months of age. The mdx mouse carries a nonsense

Authorship note: CHH and NBW contributed equally to this work.

Conflict of interest: DD is a member of the scientific advisory board of and an equity holder in Solid Biosciences LLC. DD and YY are inventors on patents that were licensed to Solid Biosciences LLC (US patent 7,892,824; Chinese patent ZL 200880002602.3; Japanese patent 5575486; Hong Kong patent HK1143326; German patent 602008028126.4; Great Britain patent GB2125006; Irish patent IE2125006; French patent FR2125006). The Duan lab has received research support unrelated to this project from Solid Biosciences LLC. CHH, DD, NBW, and YY have filed a patent application related to the findings described in this paper (US provisional application 62/661,391). CAG has filed patent applications related to genome editing for Duchenne muscular dystrophy (international patent application PCT/US2013/038536; US provisional applications 61/839127, 61/904911, 62/260,712, 62/332,297, 62/363,888). CAG is an advisor to and receives research support from Sarepta Therapeutics Inc. CAG and CEN are inventors on patent applications related to genome editing (international patent application PCT/US14/41190; US provisional applications 61/803254, 61/981575, 62/082,315, 62/113,569, 62/230,931, 62/195,680, 62/209,466, 61/719,276). Solid Biosciences LLC has optioned disclosures 6UMC049 and 17UMC006, which include patent application PCT/US2017/038418.

Submitted: August 20, 2018
Accepted: October 31, 2018
Published: December 6, 2018

Reference information:
JCI Insight. 2018;3(23):e124297.
https://doi.org/10.1172/jci.insight.124297.

mutation in exon 23 of the dystrophin gene (12). This mutation can be removed by codelivery of an AAV. Cas9 vector that expresses *Staphylococcus aureus* Cas9 and an AAV.gRNA vector that directs Cas9 to introns 22 and 23 (2). AAV-9 is a well-established AAV serotype for robust skeletal muscle and cardiac transduction in mdx mice (13, 14). We first used a method that has shown success in short-term studies (7). To our surprise, this method yielded nominal CRISPR editing in skeletal muscle, limited dystrophin restoration in the heart, and no improvement in cardiac histology and hemodynamic function. Subsequent analysis showed similar levels of Cas9 expression in the heart and skeletal muscle. Interestingly, vector genome quantification showed a disproportionate reduction of the gRNA vector by a large margin. To determine whether depletion of the gRNA vector contributed to the poor outcome, we repeated the study with an increased dose of the gRNA vector. This modification not only significantly enhanced dystrophin expression in the heart, but also resulted in body-wide dystrophin restoration in skeletal muscle. Importantly, it reduced fibrosis in the heart and skeletal muscle, significantly increased skeletal muscle force, and enhanced cardiac hemodynamic function. Additional studies suggest that vector dose alteration had minimal effect on dystrophin restoration on local AAV CRISPR therapy. These results identify gRNA vector depletion as a hurdle for systemic AAV CRISPR therapy. Increasing gRNA vector dose is necessary to achieve sustained skeletal muscle and heart rescue in DMD.

Results

Loss of the gRNA vector limited long-term systemic AAV CRISPR therapy in mdx mice. Effective DMD treatment requires persistent dystrophin restoration and functional improvements in both skeletal and cardiac muscle. To determine whether systemic AAV CRISPR therapy can lead to long-lasting protection for DMD, we coinjected the Cas9 and gRNA vectors into six 6-week-old male mdx mice at the dose of 7.2×10^{12} viral genome particles (vg)/mouse and 3.6×10^{12} vg /mouse, respectively, via the tail vein (study 1 in Supplemental Table 1; supplemental material available online with this article; https://doi.org/10.1172/jci.insight.124297DS1). One mouse was harvested at 8 months of age to evaluate dystrophin restoration. By immunostaining and Western blot, robust dystrophin expression was detected in the heart but not in skeletal muscle (Supplemental Figure 1). Remaining mice were harvested at 18 months of age. Likewise, dystrophin expression was barely detected in skeletal muscle (Figure 1, A–D; Supplemental Figure 1B; and Supplemental Figure 2), but widespread dystrophin expression was found throughout the entire heart cross-section by immunostaining (Figure 1A and Supplemental Figure 2A). On Western blot, cardiac dystrophin reached approximately 5% of the WT level (Figure 1, C and D; Supplemental Figure 1B; Supplemental Figure 3; and Supplemental Figure 4). Consistent with immunostaining and Western blot results, nominal levels of the edited dystrophin transcript were detected in skeletal muscle (Figure 1E and Supplemental Figure 5). No difference was noted in the total dystrophin transcript levels between treated and untreated mdx mice (Supplemental Figure 6). We next examined whether cardiac dystrophin expression improved heart structure and function (Figure 1F and Supplemental Tables 2–4). Significant improvement was detected in ECG but not in other cardiac endpoints (Figure 1F and Supplemental Tables 2–4). To determine whether long-term Cas9 expression increased off-target editing, we performed deep sequencing on both target sites and predicted off-target sites. Despite the high levels of indel formation at the target sites, we did not find significant editing in the predicted top off-target sites (Figure 1G). Histological examination of major internal organs also showed no obvious abnormality (Supplemental Figure 7).

To understand the mechanism(s) underlying poor dystrophin restoration, we quantified the levels of Cas9 expression and vector genome persistence at 18 months after treatment (Figure 1, H and I, and Supplemental Figures 8–10). Similar levels of Cas9 expression were observed at the cDNA and protein levels between the heart and skeletal muscle, although the Cas9 vector genome in the heart was significantly higher than that in skeletal muscle (Figure 1, H and I, and Supplemental Figure 8). Most of the AAV vector genome was found in the liver (Supplemental Figure 9) (13, 15–17). Interestingly, the gRNA vector genome was significantly depleted compared with that of the Cas9 vector genome in every tissue examined (Figure 1I and Supplemental Figures 9 and 10). The Cas9 vector–to–gRNA vector genome copy ratio reached approximately 12–14 in muscles and internal organs (Supplemental Figure 10). This was approximately 6- to 7-fold higher than the expectation based on the vector dose at the time of AAV injection (Supplemental Table 1).

Increasing the gRNA vector dose resulted in long-lasting dystrophin restoration and function improvement in striated muscles throughout the body. With recognition of the preferential gRNA vector depletion, we repeated the study using 1×10^{13} vg/mouse of the Cas9 vector and 3×10^{13} vg/mouse of the gRNA vector in 6-week-old

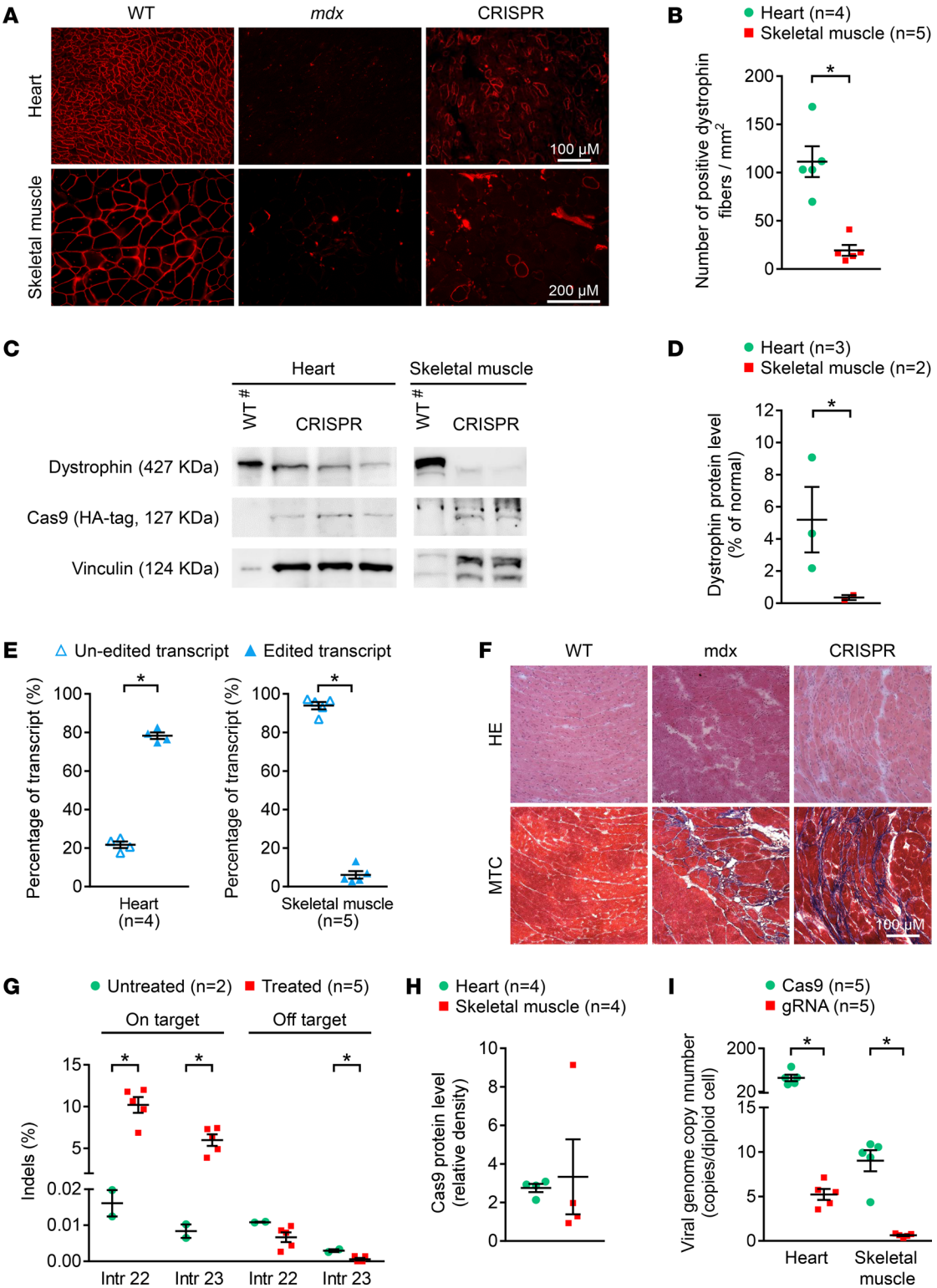

Figure 1. Long-term systemic AAV CRISPR therapy in mdx mice is associated with disproportional depletion of the gRNA vector genome. Systemic AAV-9 CRISPR therapy was performed in 6-week-old male mdx mice at the dose of 7.2×10^{12} vg/mouse and 3.6×10^{12} vg/mouse for the Cas9 and gRNA vectors, respectively. Mice were evaluated at 18 months of age. (**A**) Representative dystrophin immunostaining photomicrographs from WT, mdx, and CRISPR-treated mdx mice. Scale bar: 100 μm (top); 200 μm (bottom). (**B**) Quantification of dystrophin-positive myofibers. (**C**) Representative dystrophin Western blot from WT and CRISPR-treated mice. (**D**) Quantification of dystrophin Western blot. (**E**) Quantification of edited and unedited dystrophin transcripts. (**F**) Representative H&E and Masson trichrome (MTC) staining of the heart. Scale bar: 100 μm. (**G**) Deep sequencing quantification of indels in untreated and CRISPR-treated mdx mice. (**H**) Quantification of Cas9 protein expression. (**I**) Quantification of the AAV genome copy number. For **B**, **E**, and **H**, statistical analyses were performed using Mann-Whitney test. For **D**, unpaired *t* test was used. For **G** and **I**, multiple *t* tests was used for statistical analysis. $^*P < 0.05$. #Loading in this lane was at one-sixth the volume of that in other lanes. The quadriceps or gastrocnemius muscle was used to generate the skeletal muscle data shown in the figure.

mdx mice (studies 2 and 3 in Supplemental Table 1). We first repeated the study in male mdx mice (study 2 in Supplemental Table 1). At the 18 months of age, we observed widespread dystrophin expression by immunostaining in both the hearts and skeletal muscle in treated mice (Figure 2A and Supplemental Figure 11). On Western blot, dystrophin reached approximately 20% in the heart and approximately 2% in skeletal muscle (Figure 2, C and D). Consistent with these results, we detected a significant increase of the total dystrophin transcript in the hearts of treated mice (Figure 2E). 80% of these transcripts were corrected by CRISPR editing (Supplemental Figure 12). In contrast to what we saw in study 1 (Figure 1E), we found that approximately 30% of dystrophin transcripts were edited in skeletal muscle in study 2 (Supplemental Figure 12). The patterns of the Cas9 vector genome distribution and Cas9 expression in heart and skeletal muscle were similar to what we saw in study 1 (Figure 1H and Supplemental Figures 8 and 13). There was also no detectable off-target editing at the computer-predicted off-target sites for these gRNAs (Supplemental Figure 14). Encouragingly, the Cas9 vector–to–gRNA vector genome copy number ratio was now close to 1 in every tissue we examined (Figure 2F and Supplemental Figure 10B). Next, we evaluated muscle histology and skeletal muscle strength (Figure 2, G–J; Supplemental Figure 15; and Supplemental Table 5). Fibrosis was reduced in both skeletal muscle and the heart (Figure 2, G and H, and Supplemental Figures 15 and 16). Pathologic muscle hypertrophy in mdx mice was mitigated (Supplemental Table 5). Specific twitch and tetanic forces were significantly enhanced (Figure 2I). CRISPR therapy also significantly improved resistance to eccentric contraction-induced force drop (Figure 2J).

To validate the findings in male mdx mice, we performed study 3 using female mdx mice (study 3 in Supplemental Table 1). Similar to what we saw in male mice in study 2 (Figure 2, A–D, and Supplemental Figure 11), body-wide dystrophin expression was observed in all striated muscles in CRISPR-treated female mdx mice at 18 months of age (Figure 3, A–D, and Supplemental Figure 17). Quantification of dystrophin Western blot showed approximately 9% expression in the heart and approximately 4% expression in skeletal muscle (Figure 3D and Supplemental Figure 4). These values are significantly higher than what we observed in study 1 (Figure 1D and Supplemental Figure 4). Treatment significantly increased the total dystrophin transcript level in the heart, of which approximately 80% was edited (Figure 3E). In skeletal muscle, edited transcripts accounted for half of the total dystrophin transcripts (Figure 3E). Similar patterns of Cas9 expression, Cas9 vector genome, and on/off-target editing were found in CRISPR-treated female mdx mice (Supplemental Figures 18 and 19). Consistent with the findings in male mice in study 2 (Figure 2F and Supplemental Figure 10B), the copy number of the Cas9 and gRNA vector reached similar levels in every tissue examined (Figure 3F and Supplemental Figure 10C). By histological examination, we detected a clear reduction of muscle and heart fibrosis (Figure 3, G and H, and Supplemental Figures 20 and 21). Cardiac anatomy was unremarkable, but improvement was found in ECG (Supplemental Tables 6 and 7). Failure to enhance heart pump function was a major concern of study 1 (Supplemental Table 4). We found a significant improvement of the end-systolic volume and ejection fraction in CRISPR-treated mice (Figure 3I). A trend of improvement was also observed in other hemodynamic parameters (Supplemental Table 8).

Manipulation of the vector dose did not influence dystrophin restoration in mdx muscle in local CRISPR therapy. To determine whether the vector ratio affected the outcome of intramuscular CRISPR therapy, we injected the Cas9 and gRNA vectors at different ratios into the tibialis anterior muscles of 6-week-old mdx mice (Supplemental Table 9). No appreciable dystrophin restoration was detected when only the Cas9 or gRNA vector was injected (Figure 4, A and B, and Supplemental Figure 22). Coinjection of both vectors at the dose of 1×10^{11} vg/vector resulted in approximately 20% dystrophin-positive myofibers. Interestingly, tripling the gRNA vector yielded similar levels of dystrophin restoration (Figure 4, A and B, and Supplemental Figure 22). Western blot confirmed immunostaining results (Figure 4, C and D). Vector genome quantification did not reveal preferential loss of the gRNA vector (Figure 4E).

Discussion

Targeted correction of mutated genes with AAV CRISPR is being actively pursued in preclinical studies to treat inherited diseases that affect multiple tissues/organs, such as DMD (18–20). A therapy that can result in sustained disease amelioration with a one-time administration would be highly preferred. Despite the need, long-term protection from AAV CRISPR therapy has never been demonstrated. Here, we tested whether a single intravenous AAV-9 CRISPR therapy in young mdx mice can result in long-lasting disease rescue in the commonly used mdx model. We initially hypothesized that a high amount of the Cas9 vector might result in more efficient cutting of the mutated genome and, hence, better disease rescue (7). Surprisingly, we observed

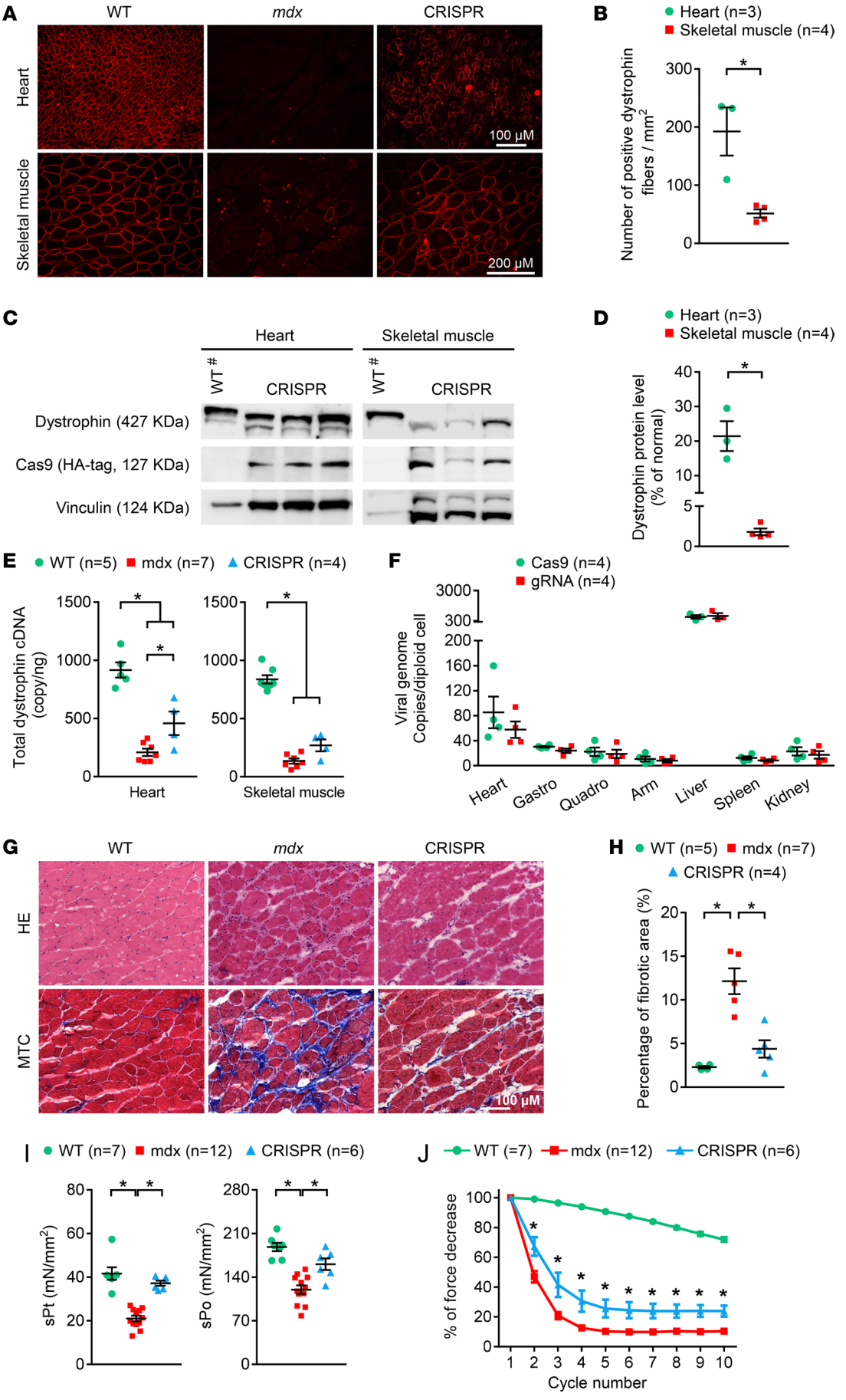
A
WT
mdx
CRISPR
Heart
Skeletal muscle
100 μM
200 μM
B
Heart (n=3)
Skeletal muscle (n=4)
Number of positive dystrophin fibers / mm2
C
Heart
Skeletal muscle
WT #
CRISPR
Dystrophin (427 KDa)
Cas9 (HA-tag, 127 KDa)
Vinculin (124 KDa)
D
Heart (n=3)
Skeletal muscle (n=4)
Dystrophin protein level (% of normal)
E
WT (n=5)
mdx (n=7)
CRISPR (n=4)
Total dystrophin cDNA (copy/ng)
Heart
Skeletal muscle
F
Cas9 (n=4)
gRNA (n=4)
Viral genome Copies/diploid cell
Heart
Gastro
Quadro
Arm
Liver
Spleen
Kidney
G
WT
mdx
CRISPR
HE
MTC
100 μM
H
WT (n=5)
mdx (n=7)
CRISPR (n=4)
Percentage of fibrotic area (%)
I
WT (n=7)
mdx (n=12)
CRISPR (n=6)
sPt (mN/mm2)
sPo (mN/mm2)
J
WT (=7)
mdx (n=12)
CRISPR (n=6)
% of force decrease
Cycle number

Figure 2. Systemic AAV CRISPR therapy resulted in sustained skeletal muscle function improvement in mdx mice. Systemic AAV-9 CRISPR therapy was performed in 6-week-old male mdx mice at the dose of 1×10^{13} vg/mouse and 3×10^{13} vg/mouse for the Cas9 and gRNA vectors, respectively. Mice were evaluated at 18 months of age. (**A**) Representative dystrophin immunostaining photomicrographs from WT, mdx and CRISPR-treated mdx mice. Scale bar: 100 μm (top); 200 μm (bottom). (**B**) Quantification of dystrophin-positive myofibers. (**C**) Representative dystrophin Western blot from WT and CRISPR-treated mice. (**D**) Quantification of dystrophin Western blot. (**E**) Quantification of total dystrophin transcripts. (**F**) Quantification of the AAV genome copy number. (**G**) Representative skeletal muscle H&E and Masson trichrome (MTC) staining. Scale bar: 100 μm. (**H**) Quantification of fibrosis in skeletal muscle. (**I**) Specific twitch (sPt) and tetanic force (sPo). (**J**) Eccentric contraction profile. Statistical analyses were done using following tests: **B** and **D**, 2-tailed Student's *t* test; **F**, multiple *t* tests (statistical analysis was only performed between the Cas9 data and the gRNA data in each organs; we did not compare data from different organs); **E**, **H**, and **I**, 1-way ANOVA; and **J**, 2-way ANOVA. $^*P < 0.05$. #Loading in this lane was at one-fourth the volume of that in other lanes. The quadriceps or gastrocnemius muscle was used to generate the skeletal muscle data shown in the figure.

poor dystrophin restoration and minimal attenuation of dystrophic signs at 18 months of age (Figure 1, A–D; Supplemental Figures 1–4; and Supplemental Tables 2–4). Intriguingly, we also detected disproportional depletion of the gRNA vector genome (Figure 1I and Supplemental Figures 9 and 10). To determine whether the gRNA vector loss underlay the poor outcome, we repeated the study with increased amount of the gRNA vector in a larger cohort of mice. In humans, dystrophin deficiency affects both males and females (21). In mdx mice, males display more severe skeletal muscle disease, while females show more severe cardiomyopathy (22, 23). To more stringently test the treatment effect, we included males to study skeletal muscle rescue and females to study cardiac rescue in new experiments (studies 2 and 3 in Supplemental Table 1). In contrast to what we saw in our first study (study 1 in Supplemental Table 1), the revised dose regimen significantly increased dystrophin expression (Figure 2, A–D; Figure 3, A–D; and Supplemental Figures 4, 11, and 17). Importantly, improved dystrophin restoration greatly mitigated muscle fibrosis and resulted in physiologically significant enhancement in skeletal muscle and heart function (Figure 2, G–J; Figure 3, G–I; Supplemental Figures 15, 16, 20, and 21; and Supplemental Tables 5, 7, and 8).

Short-term dual AAV CRISPR therapy has been performed in a variety of animal models by many laboratories. In these studies, often equal amounts of the Cas9 and gRNA vectors are coinjected and therapeutic effect is examined a few weeks later to establish proof-of-principle. In the context of DMD, a 1:1 or 2:1 ratio of the Cas9 to gRNA vector has been shown to induce dystrophin expression in skeletal and cardiac muscle after systemic delivery in newborn and young mice (1–3, 7, 10, 11). We used a dose similar to those published before ($\geq 2 \times 10^{12}$ vg/vector/adult mouse) at a Cas9-to-gRNA vector ratio of 2:1 (Supplemental Table 1). Given the need for long-term therapy, we examined dystrophin expression at 8 and 18 months of age. Unexpectedly, we were only able to detect expression of the edited dystrophin protein in the heart at a level insufficient to reduce myocardial fibrosis or enhance blood pumping function (Figure 1; Supplemental Figures 1, 2, and 4; and Supplemental Tables 2–4). Minimal dystrophin restoration was found in skeletal muscle (Figure 1, A–D, and Supplemental Figures 1 and 2).

To better understand this observation, we quantified the dystrophin transcript, Cas9 expression, and the vector genome copy number. Similar to the protein results, edited transcripts were only found in the heart (Figure 1E). However, the total dystrophin transcript level was not increased, suggesting that the limited editing did not overcome nonsense-mediated decay in mdx mice (Supplemental Figure 6) (24). Despite the detection of significantly more Cas9 vectors in the heart than in skeletal muscle (Supplemental Figure 8), no significant difference was noticed in regards to Cas9 expression between the heart and skeletal muscle (Figure 1H and Supplemental Figure 8). This result was consistent with reports that the cytomegalovirus promoter has different activity in different cell types (25). Importantly, this result excluded the Cas9 level as the cause of poor skeletal muscle editing. Next, we quantified the amount of the AAV vector genome. The copy number of the Cas9 vector was significantly higher than that of the gRNA vector in all tissues (Figure 1I and Supplemental Figure 9). Remarkably, it greatly exceeded the 2-fold dose difference at the time of AAV injection (Supplemental Figure 10 and Supplemental Table 1). The gRNA vector genome copy number per myonucleus was 0.33 ± 0.04 in upper arm muscles, 0.63 ± 0.09 in quadriceps, and 0.77 ± 0.16 in gastrocnemius (Supplemental Figure 9). Hence, a large proportion of skeletal myonuclei had no gRNA vector. This correlated well with the editing failure seen in skeletal muscle (Figure 1E). The reason for the preferential depletion of the gRNA vector genome is unclear, but it may likely relate to the hairpin structure in this vector. The cruciform configuration is known to compromise DNA stability (26).

The discovery of the selective gRNA genome loss suggests that the gRNA vector dose may represent an important limiting factor for dual AAV CRISPR therapy. To investigate this possibility, we conducted two new studies using a higher dose of the gRNA AAV vector. Since our first study revealed an approximately 6- to 7-fold greater loss of the gRNA vector than expected, we increased the gRNA AAV dose by 6-fold

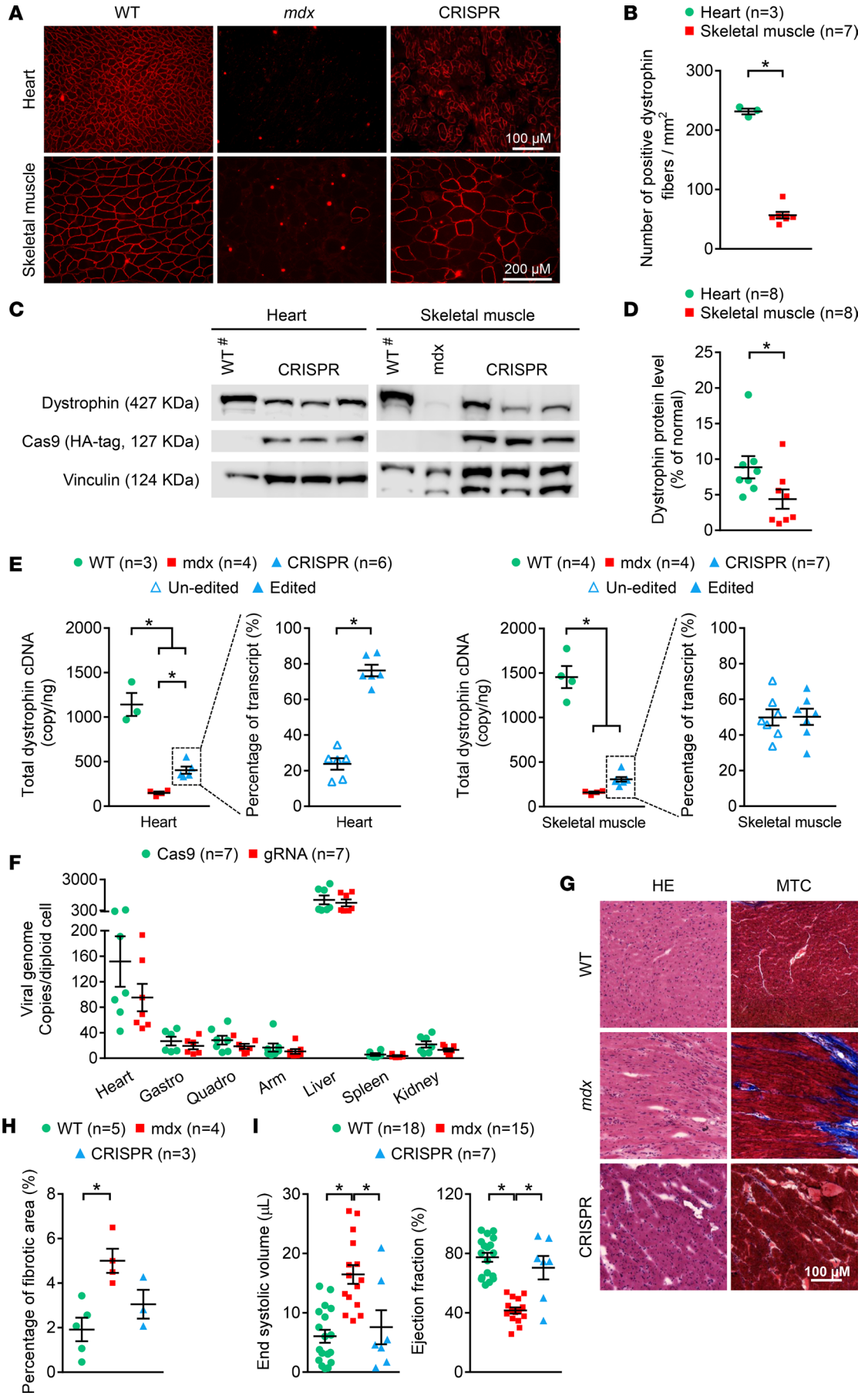
A
WT
mdx
CRISPR
Heart
Skeletal muscle
100 μM
200 μM
B
Heart (n=3)
Skeletal muscle (n=7)
Number of positive dystrophin fibers / mm2
C
Heart
Skeletal muscle
WT #
CRISPR
mdx
Dystrophin (427 KDa)
Cas9 (HA-tag, 127 KDa)
Vinculin (124 KDa)
D
Heart (n=8)
Skeletal muscle (n=8)
Dystrophin protein level (% of normal)
E
WT (n=3) mdx (n=4) CRISPR (n=6)
Un-edited Edited
Total dystrophin cDNA (copy/ng)
Percentage of transcript (%)
Heart
WT (n=4) mdx (n=4) CRISPR (n=7)
Skeletal muscle
F
Cas9 (n=7) gRNA (n=7)
Viral genome Copies/diploid cell
Heart
Gastro
Quadro
Arm
Liver
Spleen
Kidney
G
HE
MTC
WT
mdx
CRISPR
100 μM
H
WT (n=5) mdx (n=4)
CRISPR (n=3)
Percentage of fibrotic area (%)
I
WT (n=18) mdx (n=15)
CRISPR (n=7)
End systolic volume (μL)
Ejection fraction (%)

Figure 3. Systemic AAV CRISPR therapy resulted in cardiac function improvement in mdx mice for 18 months. Systemic AAV-9 CRISPR therapy was performed in 6-week-old female mdx mice at the dose of 1×10^{13} vg/mouse and 3×10^{13} vg/mouse for the Cas9 and gRNA vectors, respectively. Mice were evaluated at 18 months of age. (**A**) Representative dystrophin immunostaining photomicrographs from WT, mdx, and CRISPR-treated mdx mice. Scale bar: 100 μm (top); 200 μm (bottom). (**B**) Quantification of dystrophin-positive myofibers. (**C**) Representative dystrophin Western blot from WT and CRISPR-treated mice. (**D**) Quantification of dystrophin Western blot. (**E**) Quantification of total, edited, and unedited dystrophin transcripts. (**F**) Quantification of the AAV genome copy number. (**G**) Representative heart H&E and Masson trichrome (MTC) staining. Scale bar: 100 μm. (**H**) Quantification of fibrosis in the heart. (**I**) Quantitative evaluation of the end-systolic volume and ejection fraction by cardiac catheterization. Statistical analyses were done using following tests: **B** and **E** (2-group analyses), Mann-Whitney test; **D**, 2-tailed Student's *t* test; **F**, multiple *t* tests (statistical analysis was only performed between the Cas9 data and the gRNA data in each organs; we did not compare data from different organs); and **H** and **I**, 1-way ANOVA. $^*P < 0.05$. #Loading in this lane was at one-fourth the volume of that in other lanes. The quadriceps or gastrocnemius muscle was used to generate the skeletal muscle data shown in the figure.

in new studies to reach a final Cas9-to-gRNA vector ratio of 1:3 (Supplemental Table 1). Consistent with the first study, similar levels of Cas9 protein and transcript were observed in the heart and skeletal muscle in new studies (Supplemental Figures 13 and 18). Further, the gRNA vector remained less than expected. However, the ratio of the Cas9-to-gRNA vector was now balanced in tissues harvested at 18 months of age (Figure 2F, Figure 3F, and Supplemental Figure 10). The gRNA vector genome copy number per myonucleus now reached approximately 10–30 in skeletal muscle (Figure 2F and Figure 3F).

The benefit of the new dosing regime was clearly revealed by dystrophin mRNA quantification, immunostaining, and Western blot. In the heart, the total dystrophin transcript level was significantly increased compared with that in untreated mdx mice, suggesting an effective inhibition of nonsense-mediated decay (Figure 2E and Figure 3E). Compared with that of study 1 (Figure 1, A–D, and Supplemental Figure 4), the dystrophin protein level was doubled or more than doubled in terms of the dystrophin-positive cell number in heart cross-sections and the total dystrophin level in heart lysates (Figure 2, A–D; Figure 3, A–D; and Supplemental Figure 4). In skeletal muscle, dystrophin expression increased from barely detectable in study 1 (Figure 1, A–D, and Supplemental Figures 1 and 2) to body-wide restoration (Supplemental Figure 11B and Supplemental Figure 17B), reaching approximately 2%–5% on Western blot (Figure 2, C and D, and Figure 3, C and D) in studies 2 and 3.

Fibrosis is a major pathologic presentation of dystrophic muscle. Consistent with the observed increase in dystrophin expression, we detected a clear reduction of muscle fibrosis in both skeletal and cardiac muscle in studies 2 and 3 (Figure 2, G and H; Figure 3, G and H; and Supplemental Figures 15, 16, 20, and 21). A critical goal of DMD gene therapy is to restore muscle and heart function, because only functional rescue can be directly translated to life quality improvement. To more stringently evaluate physiological changes associated with the new dose regime, we intentionally assayed skeletal muscle force in treated male mice, despite the facts that (a) male mdx mice display more severe skeletal muscle force deficits than female mdx mice (22) and (b) the dystrophin level on Western blot was relatively lower in skeletal muscle of treated male mice than that of treated female mice (Figure 2, C and D, and Figure 3, C and D). For similar reasons, we also intentionally assayed heart function in treated female mice (Figure 2, B and D, and Figure 3, B and D) (23). The extensor digitorum longus (EDL) muscle is one of most representative muscles commonly used for measuring skeletal muscle function in mdx mice (27, 28). We found that the modified AAV CRISPR therapy significantly mitigated pathological muscle hypertrophy and significantly increased specific twitch and tetanic forces (Figure 2, I and J, and Supplemental Table 5). Importantly, it significantly mitigated the rapid force drop induced by eccentric contraction, a characteristic feature of mdx mice (Figure 2J). To study heart function, we measured cardiac electrophysiology and hemodynamics by ECG and closed chest cardiac catheter assay, respectively (29). Compared with untreated mdx mice, CRISPR-treated mice showed improvement in most ECG parameters (Supplemental Table 7). On hemodynamic evaluation, a significant reduction of the end-systolic volume was detected, suggesting a prevention of pathological chamber size dilation (Figure 3I). CRISPR therapy also significantly enhanced the heart pump function, as reflected on ejection fraction measurement (Figure 3I). In addition, all other hemodynamic parameters showed a trend of improvement (Supplemental Table 8). This is in sharp contrast with what we saw in study 1, where the values of all hemodynamic parameters were essentially identical between CRISPR-treated and untreated mice (Supplemental Table 4). Collectively, by increasing the gRNA vector dose, we have achieved disease amelioration for 18 months with a single intravenous AAV CRISPR therapy.

Given the unexpected observation of gRNA vector depletion in systemically treated mice, we investigated the effect of the vector ratio on local injection. Surprisingly, increasing the Cas9-to-gRNA vector ratio from 1:1 to 1:3 did not enhance dystrophin expression (Figure 4, A–D). On vector genome quantification, we did not see preferential gRNA vector loss (Figure 4E). The Cas9-to-gRNA vector

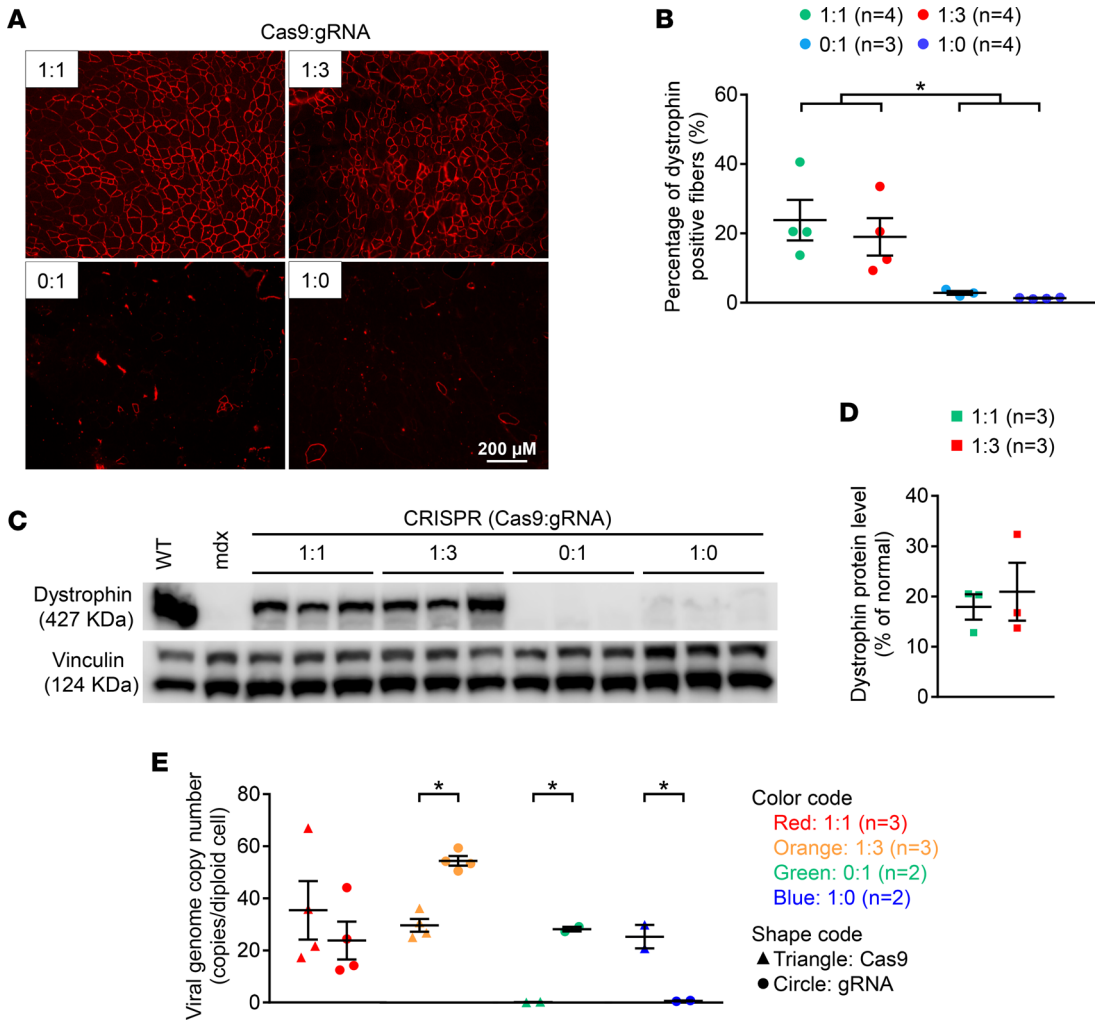

Figure 4. Increasing the gRNA AAV vector dose did not alter dystrophin expression following intramuscular AAV CRISPR therapy. The Cas9 and gRNA AAV vectors were coinjected to the tibialis anterior muscle of 6-week-old mdx mice at the Cas9 vector-to-gRNA vector ratio of 1:0 (1×10^{11} vg Cas9 only), 0:1 (1×10^{11} vg gRNA only), 1:1 (1×10^{11} vg Cas9 and 1×10^{11} vg gRNA), or 1:3 (1×10^{11} vg Cas9 and 3×10^{11} vg gRNA) and evaluated at 3 months of age. (**A**) Representative dystrophin immunostaining photomicrographs. Scale bar: 200 μm. (**B**) Quantification of dystrophin-positive myofibers. (**C**) Representative dystrophin Western blot. (**D**) Quantification of dystrophin Western blot. (**E**) Quantification of the AAV genome copy number. Statistical analyses were done using following tests: **B**, 1-way ANOVA; **D** and **E**, Mann-Whitney test. $^*P < 0.05$.

genome ratio in harvested muscle was proportional to that at injection (Figure 4E). To further validate these results, we quantified the AAV genome copy number in muscles harvested from our previously published local injection studies (2). Similarly, we did not see any evidence of selective gRNA vector degradation (Supplemental Figure 23). These results suggest that preferential gRNA vector depletion is a unique feature of systemic AAV CRISPR therapy. It should be pointed out that we observed selective depletion of the gRNA vector in long-term studies. Future short-term studies will reveal whether the loss of the gRNA vector is an acute effect following systemic delivery or a chronic process during long-term follow-up.

A frequent concern of CRISPR therapy is off-target editing. This is particularly worrisome for long-term CRISPR therapy because continuous expression of Cas9 may greatly increase the odds of cutting at unwanted sites. In all three long-term studies described in this manuscript, we did not detect significant off-target cutting at the top sites ranked by the computer algorithm (Figure 1G and Supplemental Figures 14 and 19). Our results agreed and extended findings of short-term studies (1–3, 7). Together, these data suggest that untoward indels at the locations predicted by the algorithm may not be a major risk for systemic AAV CRISPR therapy in dystrophic mice. Future studies are needed to determine whether long-term Cas9 expression can result in large deletions and complex rearrangements.

In summary, we have demonstrated for the first time to our knowledge that systemic AAV CRISPR editing can lead to long-term physiological benefits in a disease model. We also discovered a unique hurdle for long-term systemic AAV CRISPR therapy and developed a method to overcome it. Our findings open the door for using AAV CRISPR to treat any disease that requires systemic life-long mutation correction.

Methods

Study design. Our objective was to study long-term therapeutic benefits of AAV CRISPR therapy in a mouse DMD model. The sample size was determined based on previous experience. We did not use exclusion, randomization, or blinding approaches to assign animals to experimental group. Cardiac functional data from untreated normal and mdx mice also included those from our ongoing natural history study. All the data were included in the analysis. The primary endpoint was dystrophin expression. The secondary endpoints included vector genome copy number, Cas9 expression, on/off-target evaluation, and muscle and heart function. For each experiment, sample size reflected the number of independent biological replicates and is provided in related figures and tables.

Mice. Experimental mice were generated in house in a barrier facility using breeders purchased from The Jackson Laboratory. All mice were maintained in a specific pathogen–free animal care facility on a 12-hour-light (25 lux)/12-hour-dark cycle with access to food and water ad libitum.

AAV production and administration. The Cas9 and gRNA *cis*-plasmids have been published previously (2). AAV-9 vectors were generated by the transient transfection method and purified using CsCl ultracentrifugation, as we reported previously (30). Supplemental Figure 24 shows AAV titer titration results. The Cas9 and gRNA vectors were mixed thoroughly at the indicated quantity before injection. For systemic injection, AAV was delivered via the tail vein (Supplemental Table 1). For local injection, AAV was delivered directly to the tibialis anterior muscle (Supplemental Table 9).

AAV titration method. The AAV titer was determined by using SYBR green quantitative PCR. For the Cas9 AAV vector, we used a primer pair targeting bGHpA (forward, 5′-CGACTGTGCCTTCTAGTTGCC-3′; reverse, 5′-GACACCTACTCAGACAATGCGATG-3′). For the gRNA AAV vector, we used a primer pair targeting SV40pA (forward, 5′-AGCAATAGCATCACAAATTTCACAA-3′; reverse, 5′-CCAGACATGATAAGATACATTGATGAGTT-3′). The following thermocycler program was used for amplification using 7900HT Fast-Real-Time PCR System (Applied Biosystems). Samples were denatured at 95°C for 2 minutes. This initial denaturation was followed by 40 cycles at 95°C for 15 seconds and 60°C for 1 minute. Each sample was replicated 6–8 times for quantification. Final viral titer was calculated against a 6-point plasmid standard series representing 1×10^6 vg/μl to 1×10^{11} vg/μl at $\log_{10}$ increments for each vector (Supplemental Figure 24).

Morphological studies. Tissues were harvested at the indicated time point in liquid nitrogen-cooled 2-methylbutane in the Tissue-Plus optimal cutting temperature compound (Scigen Scientific). General histology and fibrosis were examined by H&E and Masson trichrome staining, respectively. Dystrophin was detected with a rabbit polyclonal antibody against the C-terminal domain (catalog RB 9024, 1:200; Thermo Fisher Scientific). Slides were viewed using a Nikon E800 fluorescence microscope. Photomicrographs were taken with a Leica DFC7000 camera.

Western blot. Proteins from heart and skeletal muscle were extracted according to our published protocol (31). Dystrophin was detected with a rabbit polyclonal antibody against the C-terminal domain (catalog RB 9024, 1:500, Thermo Fisher Scientific). Cas9 was detected with a rat monoclonal antibody against the HA tag (catalog 1-867-423, 1:500, Roche). Vinculin was used as a loading control and was detected with a rabbit polyclonal antibody (catalog ab155120, 1:2000, Abcam). Signal was detected using Clarity Western ECL substrate (Bio-Rad) and visualized using the Li-COR Odyssey imaging system. In experiments shown in Supplemental Figure 4, we used infrared fluorescence dye–conjugated secondary antibodies (LI-COR Biotechnology). Densitometry quantification was performed using the Li-COR Image Studio version 5.0.21 software (https://www.licor.com). The relative intensity of the protein was normalized to the corresponding vinculin band in the same blot and further normalized to the WT control.

Vector genome copy number quantification. Genomic DNA was extracted from OCT-embedded tissues. DNA concentration was determined using the Qubit dsDNA high-sensitivity assay kit (Thermo Fisher Scientific). The vector genome copy number was quantified by TaqMan PCR using the TaqMan Universal PCR master mix (Thermo Fisher Scientific) and custom-designed primers and probes (Supplemental Table 10). The threshold cycle value of each reaction was converted to the vector genome copy number by measuring against the copy number standard curve of the known amount of the *cis*-plasmid.

Dystrophin transcript quantification. RNA was extracted from tissues preserved in RNA later (Thermo Fisher Scientific) using the RNeasy Fibrous Tissue kit (Qiagen). The cDNA was generated using the Superscript IV Kit (Thermo Fisher Scientific) and quantified using the Qubit ssDNA assay kit (Thermo Fisher Scientific). The dystrophin transcript was quantified by digital droplet PCR in the QX200 ddPCR system (Bio-Rad) using ddPCR supermix (Bio-Rad). Primers and probes for the junctions of exon 22–23, 22–24, and 24–25 are described in Supplemental Figure 5 and Supplemental Table 10. The data were reported as the transcript copy per ng of cDNA used in the reaction.

Analysis of on- and off-target gene editing. On- and off-target cutting was analyzed using DNA extracted from flash frozen livers according to our previously published protocol (2). Primers used for deep sequencing are listed in Supplemental Table 11. Analysis was performed with CRISPResso using a 5-bp window from the expected DSB (32).

Skeletal muscle function assay. EDL muscle function was evaluated ex vivo using our published protocols (27, 28). Muscle force was evaluated with a 305B dual-mode servomotor transducer using the Dynamic Muscle Control software (Aurora Scientific). Data were analyzed using the Dynamic Muscle Analysis (DMA) software (Aurora Scientific). The specific muscle force was calculated by dividing the absolute muscle force with the muscle cross-sectional area (CSA). Muscle CSA was calculated according to the following equation: CSA = (muscle mass)/(muscle density × length ratio × optimal muscle length). Muscle density is 1.06 g/cm^3 (33). The length ratio is 0.44 for the EDL muscle (34, 35).

ECG and left ventricular hemodynamic assay. A 12-lead ECG assay was performed using a system from AD Instruments as previously published (36, 37). The ECG parameters were analyzed using ECG analysis module in Lab Chart software. The Q wave amplitude was determined using the lead I tracing. Other parameters were analyzed using the lead II tracing. The QTc interval was determined by correcting the QT interval with the heart rate as described by Mitchell et al. (38). The cardiomyopathy index was calculated by dividing the QT interval by the PQ segment (39). Left ventricular hemodynamics was evaluated with a closed chest approach using the Millar ultraminiature pressure–volume catheter (29, 37). Data were analyzed with the PVAN software (Millar Instruments). Detailed protocols are available at the Parent Project Muscular Dystrophy standard operating protocol web site (https://www.parentprojectmd.org/research/for-researchers-industry/resources/standard-operating-procedures-for-duchenne-animal-models/) (40).

Statistics. Data are presented as mean ± SEM. The sample size mentioned refers to the number of animals. For biochemical and molecular assays, 2–3 measurements were conducted in each assay for each animal. The average from these measurements was reported as the data for each animal. One-way ANOVA or two-way ANOVA with Tukey's multiple comparison was performed for statistical analysis for more than 2 group comparisons. Unpaired *t* test (2 tailed) or Mann-Whitney test was used for 2 group comparisons. The statistical method used for each analysis is indicated in the figure legends. All statistical analyses were performed using GraphPad PRISM software version 7.0. $P < 0.05$ was considered statistically significant.

Study approval. All animal experiments were approved by the University of Missouri animal care and use committee.

Author contributions

CHH, NBW, NNY, SC, CAG, and DD designed study. CHH, NBW, CEN, LPW, YY, JAL, TBL, AD, KZ, GJJ, MEN, XP, and KK performed research. CHH, NBW, LPW, and SC contributed new reagents or analytic tools. CHH, NBW, CEN, LPW, NNY, SC, CAG, and DD analyzed data. CHH, NBW, and DD wrote the paper. CHH, NBW, CEN, LPW, NNY, SC, CAG, and DD edited paper. All authors approved submission.

Acknowledgments

We thank Jim Wilson for providing the AAV-9 packaging plasmid. We thank Alex Hinken, Matt Burke, Taylor Klimt, Samantha Metzger, Courtney Harris, Mathew Pulcine, Cobi Bissell, Benjamin Schneider, Thomas Cassimatis, and Sean Duan for technical assistance. We thank the Bond Life Sciences Center at the University of Missouri for the use of the ddPCR machine. This work was supported by grants from the NIH (AR-69085 to CAG and DD; GM-063732 and GM-117059 to SC), the Intramural Research Program of the NIH National Center for Advancing Translational Sciences (to NNY and CHH), the Department of Defense (MD15-1-0469 to CAG; MD150133 to DD and CAG), Hope for Javier (to DD), the Jackson Freel DMD Research Fund (to DD), the Muscular Dystrophy Association (MDA277360 to CAG), and the Duke

Coulter Translational Partnership (to CAG). CEN was supported by a Hartwell Foundation Postdoctoral Fellowship. MEN is a predoctoral fellow supported by Hope for Javier.

Address correspondence to: Dongsheng Duan, Department of Molecular Microbiology and Immunology, The University of Missouri School of Medicine, One Hospital Drive M609, MSB, Columbia, Missouri 65212, USA. Phone: 573.884.9584; Email: duand@missouri.edu.

1. Long C, et al. Postnatal genome editing partially restores dystrophin expression in a mouse model of muscular dystrophy. *Science*. 2016;351(6271):400–403.
2. Nelson CE, et al. In vivo genome editing improves muscle function in a mouse model of Duchenne muscular dystrophy. *Science*. 2016;351(6271):403–407.
3. Tabebordbar M, et al. In vivo gene editing in dystrophic mouse muscle and muscle stem cells. *Science*. 2016;351(6271):407–411.
4. Ousterout DG, Kabadi AM, Thakore PI, Majoros WH, Reddy TE, Gersbach CA. Multiplex CRISPR/Cas9-based genome editing for correction of dystrophin mutations that cause Duchenne muscular dystrophy. *Nat Commun*. 2015;6:6244.
5. Wojtal D, et al. Spell Checking Nature: Versatility of CRISPR/Cas9 for developing treatments for inherited disorders. *Am J Hum Genet*. 2016;98(1):90–101.
6. Xu L, et al. CRISPR-mediated genome editing restores dystrophin expression and function in mdx mice. *Mol Ther*. 2016;24(3):564–569.
7. Bengtsson NE, et al. Muscle-specific CRISPR/Cas9 dystrophin gene editing ameliorates pathophysiology in a mouse model for Duchenne muscular dystrophy. *Nat Commun*. 2017;8:14454.
8. Young CS, et al. A single CRISPR-Cas9 deletion strategy that targets the majority of DMD patients restores dystrophin function in hiPSC-derived muscle cells. *Cell Stem Cell*. 2016;18(4):533–540.
9. Zhang Y, et al. CRISPR-Cpf1 correction of muscular dystrophy mutations in human cardiomyocytes and mice. *Sci Adv*. 2017;3(4):e1602814.
10. El Refaey M, et al. In vivo genome editing restores dystrophin expression and cardiac function in dystrophic mice. *Circ Res*. 2017;121(8):923–929.
11. Amoasii L, et al. Single-cut genome editing restores dystrophin expression in a new mouse model of muscular dystrophy. *Sci Transl Med*. 2017;9(418).
12. Sicinski P, Geng Y, Ryder-Cook AS, Barnard EA, Darlison MG, Barnard PJ. The molecular basis of muscular dystrophy in the mdx mouse: a point mutation. *Science*. 1989;244(4912):1578–1580.
13. Hakim CH, et al. A five-repeat micro-dystrophin gene ameliorated dystrophic phenotype in the severe DBA/2J-mdx model of Duchenne muscular dystrophy. *Mol Ther Methods Clin Dev*. 2017;6:216–230.
14. Duan D. Systemic delivery of adeno-associated viral vectors. *Curr Opin Virol*. 2016;21:16–25.
15. Inagaki K, et al. Robust systemic transduction with AAV9 vectors in mice: efficient global cardiac gene transfer superior to that of AAV8. *Mol Ther*. 2006;14(1):45–53.
16. Zincarelli C, Soltys S, Rengo G, Rabinowitz JE. Analysis of AAV serotypes 1-9 mediated gene expression and tropism in mice after systemic injection. *Mol Ther*. 2008;16(6):1073–1080.
17. Ghosh A, Yue Y, Shin JH, Duan D. Systemic Trans-splicing adeno-associated viral delivery efficiently transduces the heart of adult mdx mouse, a model for Duchenne muscular dystrophy. *Hum Gene Ther*. 2009;20(11):1319–1328.
18. Cox DB, Platt RJ, Zhang F. Therapeutic genome editing: prospects and challenges. *Nat Med*. 2015;21(2):121–131.
19. Zhang Y, Long C, Bassel-Duby R, Olson EN. Myoediting: Toward prevention of muscular dystrophy by therapeutic genome editing. *Physiol Rev*. 2018;98(3):1205–1240.
20. Nelson CE, Robinson-Hamm JN, Gersbach CA. Genome engineering: a new approach to gene therapy for neuromuscular disorders. *Nat Rev Neurol*. 2017;13(11):647–661.
21. Ishizaki M, Kobayashi M, Adachi K, Matsumura T, Kimura E. Female dystrophinopathy: Review of current literature. *Neuromuscul Disord*. 2018;28(7):572–581.
22. Hakim CH, Duan D. Gender differences in contractile and passive properties of mdx extensor digitorum longus muscle. *Muscle Nerve*. 2012;45(2):250–256.
23. Bostick B, Yue Y, Duan D. Gender influences cardiac function in the mdx model of Duchenne cardiomyopathy. *Muscle Nerve*. 2010;42(4):600–603.
24. Kerr TP, Sewry CA, Robb SA, Roberts RG. Long mutant dystrophins and variable phenotypes: evasion of nonsense-mediated decay? *Hum Genet*. 2001;109(4):402–407.
25. Qin JY, et al. Systematic comparison of constitutive promoters and the doxycycline-inducible promoter. *PLoS One*. 2010;5(5):e10611.
26. Varani G. Exceptionally stable nucleic acid hairpins. *Annu Rev Biophys Biomol Struct*. 1995;24:379–404.
27. Hakim CH, Li D, Duan D. Monitoring murine skeletal muscle function for muscle gene therapy. *Methods Mol Biol*. 2011;709:75–89.
28. Hakim CH, Wasala NB, Duan D. Evaluation of muscle function of the extensor digitorum longus muscle ex vivo and tibialis anterior muscle in situ in mice. *J Vis Exp*. 2013;(72):e50183.
29. Bostick B, Yue Y, Duan D. Phenotyping cardiac gene therapy in mice. *Methods Mol Biol*. 2011;709:91–104.
30. Shin JH, Yue Y, Duan D. Recombinant adeno-associated viral vector production and purification. *Methods Mol Biol*. 2012;798:267–284.
31. Wasala NB, Shin JH, Lai Y, Yue Y, Montanaro F, Duan D. Cardiac-specific expression of ΔH2-R15 mini-dystrophin normalized all electrocardiogram abnormalities and the end-diastolic volume in a 23-month-old mouse model of Duchenne dilated cardiomyopathy. *Hum Gene Ther*. 2018;29(7):737–748.
32. Pinello L, et al. Analyzing CRISPR genome-editing experiments with CRISPResso. *Nat Biotechnol*. 2016;34(7):695–697.

33. Mendez J, Keys A. Density and composition of mammalian muscle. *Metabolism*. 1960;9(2):184–188.
34. Burkholder TJ, Fingado B, Baron S, Lieber RL. Relationship between muscle fiber types and sizes and muscle architectural properties in the mouse hindlimb. *J Morphol*. 1994;221(2):177–190.
35. Brooks SV, Faulkner JA. Contractile properties of skeletal muscles from young, adult and aged mice. *J Physiol (Lond)*. 1988;404:71–82.
36. Bostick B, Shin JH, Yue Y, Duan D. AAV-microdystrophin therapy improves cardiac performance in aged female mdx mice. *Mol Ther*. 2011;19(10):1826–1832.
37. Wasala NB, Bostick B, Yue Y, Duan D. Exclusive skeletal muscle correction does not modulate dystrophic heart disease in the aged mdx model of Duchenne cardiomyopathy. *Hum Mol Genet*. 2013;22(13):2634–2641.
38. Mitchell GF, Jeron A, Koren G. Measurement of heart rate and Q-T interval in the conscious mouse. *Am J Physiol*. 1998;274(3 Pt 2):H747–H751.
39. Nigro G, Comi LI, Politano L. Electrocardiographic evaluation of the P-type stage of dystrophic cardiomyopathy. *Cardiomyology*. 1984;3:45–58.
40. Duan D, et al. Standard operating procedures (SOPs) for evaluating the heart in preclinical studies of Duchenne muscular dystrophy. *J Cardiovasc Transl Res*. 2016;9(1):85–86.